

Impact-Ionization Cooling in Laser-Induced Plasma Filaments

A. Filin,^{1,2} R. Compton,^{1,3} D. A. Romanov,^{1,2} and R. J. Levis^{1,3}

¹Center for Advanced Photonics Research, College of Science and Technology, Temple University, Philadelphia, Pennsylvania 19122, USA

²Department of Physics, Temple University, Philadelphia, Pennsylvania 19122, USA

³Department of Chemistry, Temple University, Philadelphia, Pennsylvania 19122, USA

(Received 6 May 2008; published 17 April 2009)

The ionization rates and subsequent electron dynamics for laser-induced plasma channels are measured for the noble gas series He, Ne, Ar, Kr, and Xe at 1.0 atm. The cw fluorescence emission increases superlinearly in the series from He to Xe in agreement with Ammosov-Delone-Krainov tunnel ionization calculations. The electron temperature after laser-induced plasma formation, measured by four-wave mixing, evolves from >20 eV to <1 eV kinetic energies with time constants ranging from 1 ns for He to 100 ps for Xe in agreement with an impact-ionization cooling model.

DOI: 10.1103/PhysRevLett.102.155004

PACS numbers: 52.38.Hb, 32.80.Rm, 52.35.Mw, 52.50.Jm

The interaction of intense, ultrafast lasers with noble gases has resulted in the discovery of many new phenomena including high harmonic generation [1,2] used to produce attosecond pulses [3–5], terahertz generation [6–8], laser filamentation [9,10], and the self phase modulation used to produce high bandwidth pulses [11]. Understanding each of these processes involves the excitation, ionization, and propagation of electrons in the intense laser field. For example, the dynamics of high harmonic generation have been modeled using a few simple parameters [12]. During the filamentation process, there are electron and plasma dynamics that go on long after the impulsive laser excitation, due to high pressure collective effects. In the case of laser-induced plasma, we find that the plasma dynamics (the initial electron energy distribution, the subsequent cooling, and the recombination of electrons with cations in the plasma) are controlled mainly through the electronic structure of the constituent gas atoms. In these measurements, the essence of the process is captured by the ionization potential of the atom and the ponderomotive potential of the driving laser.

The electronic dynamics of a plasma channel can be measured using four-wave mixing (FWM). In our experiment, two beams create a dynamic grating in the plasma channel electron density from which a third beam diffracts (see Fig. 1). The diffracted intensity is measured as a function of time delay after the plasma channel creation to provide a measurement of the electron temperature. A theory based on electron impact-ionization cooling in an atomic gas quantitatively captures the rates of plasma cooling and recombination after impulsive excitation.

A Ti:sapphire (1 kHz) laser was used for both the plasma generation and the FWM measurement as shown in Fig. 1. The plasma channel was generated with 350 μ J of horizontally polarized 800 nm, 80 fs laser focused into the sample chamber using a 5 cm focal length lens with beam diameter of 2 mm before the lens. The FWM was per-

formed with two 800 nm (1 nm FWHM, 1 ps) pump beams (ω_1 and ω_2) generated using a narrow band filter and a 971 nm (140 fs) beam (ω_3) generated using optical parametric amplification. The FWM beams and the plasma-generating beam were horizontally polarized and focused into the sample chamber using lenses to arrive simultaneously at the laser-induced plasma region. The FWM beams were arranged in a folded-boxCARS geometry, providing a spatially separated output signal, ω_S (centered at 680 nm). The diffracted beam was collimated and passed through a set of several apertures to a monochromator, equipped with a cooled CCD array detector. We probed the diffracted signal as a function of the delay between the laser-induced plasma and the FWM beams, denoted as τ_{14} . The signal was integrated over a 10 nm range, in a region around the spectral maximum of the ω_S signal. All gas samples were maintained at 1.0 atm for these measurements.

To probe the mechanism of laser-induced plasma formation, we first measured the fluorescence spectra of the plasma after excitation by the intense laser pulse ($\sim 5 \times 10^{14}$ W cm⁻²). The spectra presented in Fig. 2 consist of a set of sharp peaks on a broad flat background, marked as

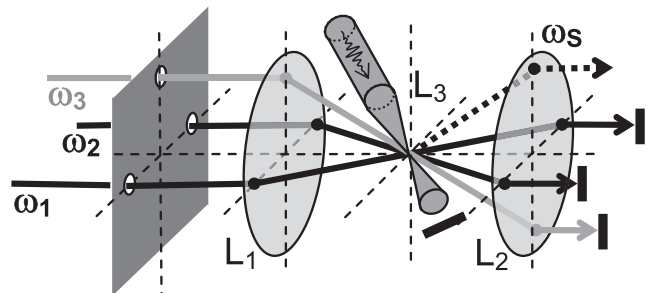


FIG. 1. Schematic of laser-induced plasma channel generation and four-wave mixing probe optics.

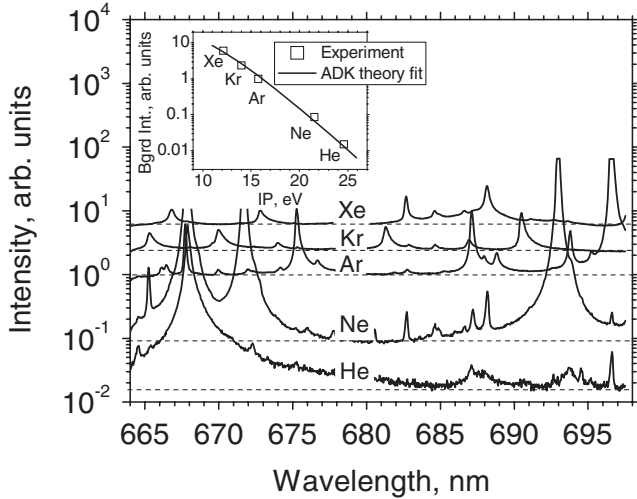


FIG. 2. Spectra of fluorescence emitted by laser-induced plasma generated after laser excitation at $\sim 5 \times 10^{14} \text{ W cm}^{-2}$. Inset shows the dependence of the fluorescence background level on the I_p of investigated gases. See text for details.

dashed lines. The sharp peaks correspond to electronic transitions in neutral atoms. The broad background is a continuum caused by the Bremsstrahlung emission. As the data presented are actually accumulated over the interpulse period of 1 ms, the background intensity is eventually proportional to the number of free electrons generated by the pulse. This intensity strongly depends on the ionization potential I_p of the gas. Doubling the I_p from Xe (12.13 eV) to He (24.59 eV) leads to a decrease in the background of nearly 3 orders of magnitude. The amount of background measured is consistent with strong-field ionization of the noble gas atoms and can be modeled using Ammosov-Delone-Krainov (ADK) theory [13], that calculates the strong-field ionization rate of an atom at any point in space time as a function of the electric field amplitude envelope, $E(\mathbf{r}, t)$.

The total number of atoms ionized by the laser pulse in the focal volume was determined by following the approach that was used in Hankin *et al.* for multiphoton ionization by a square pulse [14]. Assuming a transform-limited pulse shape with duration τ , taking into account modifications of the beam focusing geometry due to non-linearity of the refractive index [15,16] and the self-consistent plasma defocusing [17], and finally simplifying the intensity distribution in the ionization volume of length l as an axially symmetric Gaussian, we obtain the total number of singly ionized atoms, N_{tot} , as a function of the laser electric field peak amplitude, E_0 , and the species' ionization potential, I_p . The inset in Fig. 2 shows measured values of the background fluorescence vs I_p for the investigated noble gases (squares). The solid line in the inset represents the theoretical curve assuming that the fluorescence intensity is proportional to N_{tot} .

To further probe the mechanism of plasma formation, we measured the four-wave mixing signal (ω_s) as a function of time delay, τ_{14} , between the plasma formation pulse and the FWM probe pulses (see Fig. 3). The sharp spike at $\tau_{14} = 0$ is on the order of the temporal overlap between the incident beams (the plasma-generating beam and the three FWM beams). This short-lived feature arises from the interaction of the plasma beam and one particular pump beam, unlike the signal at longer time delay which requires all four beams to be present. The physics in the overlap of the pump and plasma beams is currently under investigation and is distinct from the longer-term plasma dynamics considered here. After the $\tau_{14} = 0$ spike, the FWM signal increases to a maximum value over the time interval that depends on the sample concentration, ionization potential, and the laser intensity. The temporal span between $\tau_{14} = 0$ and the maximum of the FWM signal uniformly decreases from He to Xe. The magnitude of the FWM signal at the maximum is also observed to monotonically increase from He to Xe. The FWM signal is due to scattering from the plasma continuum structure, and thus four-wave scattering will occur over a broad spectral range. The inset in Fig. 3 compares the fluorescence spectrum (gray curve) with the four-wave mixing signal (black curve) of Kr. The FWM spectrum (see inset in Fig. 3) was measured at $\tau_{14} = 1000$ ps near the temporal maximum of Kr scattering signal. The Gaussian-like shape of the FWM spectrum observed in the inset of Fig. 3 is defined by the spatial phase mismatch for fs-boxCARS [18]. To decrease the fluorescence contribution, the spectral region from 676 to

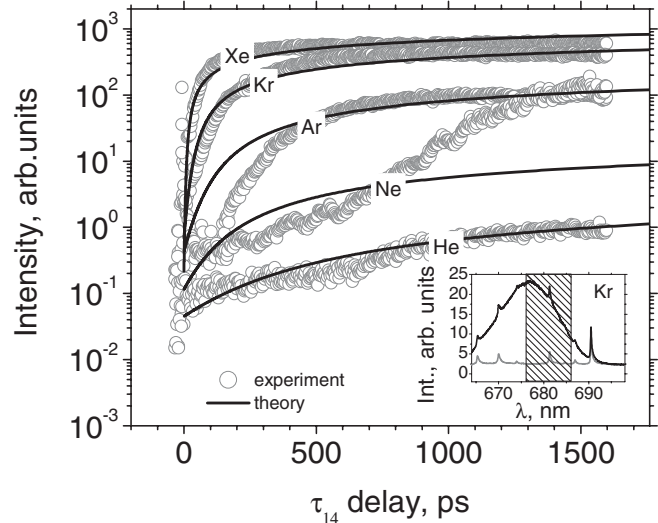


FIG. 3. Intensity of the FWM signal vs τ_{14} delay, measured at the spectral position near the maximum of the FWM signal (circles) and FWM signal intensity vs time simulated by our theoretical model (solid lines). The inset shows the FWM (black curve) and fluorescence (gray curve) spectra of Kr. The spectral region, where the time-resolved signal was accumulated, is shadowed.

686 nm was chosen for the time-resolved FWM intensity measurements. The region contains a minimal number of fluorescence peaks for all 5 investigated noble gases. Note that the fluorescence signal has a much longer time scale than the FWM signal and thus does not alter the time dependence of this latter signal within the 2 ns time interval probed in these measurements.

The evolution of the signal intensity can be understood using a three-step model where the electrons are first ionized and accelerated to the ponderomotive potential during the plasma-generating pulse, then cool mainly through inelastic collisions with neutral atoms, and finally undergo FWM based on a ponderomotive grating induced by the ω_1 and ω_3 beams. Upon the ionization and possible electron rescattering during the intense femtosecond laser pulse, considerable kinetic energy (on the order of 3.2 X ponderomotive potential) is imparted to the plasma electrons and is on the order of 20 eV for the laser intensity used here ($\sim 5 \times 10^{14}$ W cm $^{-2}$). As the electron temperature is established extremely rapidly, on subpicosecond time scale [19], we can assume that the electrons are characterized by a thermal distribution function at any step during plasma cooling. The main cooling mechanism is the energy loss on impact ionization of the remaining neutral atoms. By assuming so, we neglect both multiple ionization and impact excitation of atoms and ions. Further, we neglect plasma diffusion processes because the measurements concern plasma evolution on the picosecond time scale and tens of micrometer length scale. This process is described by coupled differential equations for the electron temperature, T , and the electron concentration, n :

$$n \frac{dT}{dt} = -\left(T + \frac{2}{3}I_p\right) \frac{dn}{dt}; \quad \frac{dn}{dt} = \nu(T)n(n_0 - n), \quad (1)$$

where n_0 is the initial density of neutral atoms. The first part of Eq. (1) concerns conservation of energy, showing that impact-ionization events occur at the expense of reducing the electron gas temperature. The second part concerns the chemical kinetics equation for the binary reaction of ionization. The ionization rate, $\nu(T)$, is determined by the dependence of the total impact-ionization cross section on the electron energy, $\sigma(E)$. Although there are asymptotic expressions for this cross section for large values of electron energy, $E \gg I_p$ and first-principles calculations for $E \ll I_p$, the area of intermediate energies, $E \sim I_p$ that is of our primary concern, remains a topic of heated discussions (see, e.g., [20–22] and references therein). For the sake of simplicity, we adopt here the widely used semiempirical Lotz approximation [23], $\sigma \propto \ln(1 + E/I_p)/(1 + E/I_p)$, that leads to

$$\nu(T) = -2\sqrt{\pi\gamma} \frac{\hbar a_B}{m} \left(\frac{Ry}{I_p}\right)^{3/2} \sqrt{\frac{I_p}{T}} Ei\left(-\frac{I_p}{T}\right) \quad (2)$$

where γ is a phenomenological parameter and $Ei(z)$ is the integral exponential. Then, the implicit solution to the

system of Eq. (1) is obtained as,

$$\int_{\theta(0)}^{\theta} \frac{\sqrt{\theta'} d\theta'}{Ei\left(-\frac{1}{\theta'}\right)(\theta' - \theta_f)} = \frac{t}{t_0}; \quad n = n(0) \frac{3\theta(0) + 2}{3\theta + 2}, \quad (3)$$

where $\theta = T/I_p$ is the dimensionless temperature, $\theta_f = [n(0)/n_0][\theta(0) + 2/3] - 2/3$, $\theta(0)$ and $n(0)$ are the initial values of the electron temperature and density (as determined by the initial pulse ionization), and the characteristic time scale for electron cooling is then $t_0 = [m/(2\sqrt{\pi\gamma\hbar a_B})](I_p/Ry)^{3/2}$.

Generally, there are two major mechanisms contributing to the four-wave mixing signal intensity in a plasma, the electron density grating due to the ponderomotive potential of the pump beams and the electron temperature grating due to local heating. For the femtosecond pulses used in our experiments, only the first mechanism is relevant, that is well described in the framework of hydrodynamic plasma equations. Following Ref. [24], the dependence of the intensity of the scattered light on the plasma parameters may be approximated as

$$I \propto \frac{\omega_p^2}{T^2} \propto \left(\frac{n(0)}{n_0}\right)^2 \frac{[3\theta(0) + 2]^2}{\theta^2(3\theta + 2)^2}. \quad (4)$$

Physically, this estimate means that to cause appreciable four-wave mixing in plasma, the ponderomotive grating modulation must counteract the thermal motion of the electrons (in the experiment, the focal-volume intensity of the three beams of the FWM scheme is on the order of 10^{11} W/cm 2 , that corresponds to about 6 meV of ponderomotive potential). This is why the FWM signal grows and saturates with the plasma cooling. Figure 3 (solid curves) shows the result of simulation of FWM intensity as a function of time. The data were fit with Eq. (4) using $\theta(0)$ for the initial plasma temperature and $n(0)/n_0$ for the initial degree of ionization. These parameters were fit for one gas, argon, where they correspond to the initial electron temperature of 20 eV (about 0.6 Up) and the initial degree of ionization of about 1.05×10^{-2} . For the remaining gases, each of the parameters was scaled according to the corresponding value of I_p , taking also into account the changes in the focusing geometry due to nonlinear refraction index and plasma defocusing. The parameter γ [proportional to the electron scattering cross section in Eq. (2)] was fit for one gas and was then scaled for the remaining gases using the known values of maximum total impact-ionization cross sections taken from [15]. With these fitting parameters, the observed growth of the FWM signal corresponds to electron cooling to approximately 800 meV.

In the measurements made on noble gases, there is a clear trend of increasing time constant for electron cooling as the ionization potential of the atom increases. The measurements and theory suggest that the lower the characteristic energy level spacing in an atom, the faster the electron distribution in the plasma channel cools. There is a

decrease in the absolute FWM intensity with increasing ionization potential. This is attributed to the lower electron density produced with increasing ionization potential as predicted by ADK ionization rate. The ADK ionization prediction is also in agreement with the measurement of the cw fluorescence from the atoms using a simple spectrometer.

The model presented for the ultrafast dynamics of laser-induced plasma channels reveals the connections among the fundamental processes of laser-induced tunnel ionization, plasma cooling dynamics of the produced plasma channel, and the residual fluorescence of the channel. The results obtained link the dynamic behavior of the underdense plasma formation with the internal degrees of freedom of the constituent species suggesting that related processes of much current interest, such as laser-induced breakdown, laser-induced ablation, and, further, atmospheric filamentation will depend sensitively on atomic and molecular constituents. This opens the way to optimizing plasma channel characteristics (bandwidth, coherence, brightness) to that desired for a particular experiment.

We acknowledge the support of DARPA Microsystems Technology Office and the National Science Foundation for this research.

[1] A. L'Huillier and P. Balcou, Phys. Rev. Lett. **70**, 774 (1993).

[2] J. J. Macklin, J. D. Kmetec, and C. L. Gordon III, Phys. Rev. Lett. **70**, 766 (1993).
[3] N. A. Papadogiannis *et al.*, Phys. Rev. Lett. **83**, 4289 (1999).
[4] M. Hentschel *et al.*, Nature (London) **414**, 509 (2001).
[5] P. M. Paul *et al.*, Science **292**, 1689 (2001).
[6] S. Tzortzakis *et al.*, Opt. Lett. **27**, 1944 (2002).
[7] K. Y. Kim *et al.*, Opt. Express **15**, 4577 (2007).
[8] C. D. Amico *et al.*, New J. Phys. **10**, 013015 (2008).
[9] A. Braun *et al.*, Opt. Lett. **20**, 73 (1995).
[10] M. Rodriguez *et al.*, Phys. Rev. E **69**, 036607 (2004).
[11] N. Akozbek *et al.*, Opt. Commun. **191**, 353 (2001).
[12] P. B. Corkum, Phys. Rev. Lett. **71**, 1994 (1993).
[13] M. V. Ammosov, N. B. Delone, and V. P. Krainov, Sov. Phys. JETP **64**, 1191 (1986).
[14] S. M. Hankin *et al.*, Phys. Rev. A **64**, 013405 (2001).
[15] H. J. Lehmeyer, W. Leupacher, and A. Penzkofer, Opt. Commun. **56**, 67 (1985).
[16] J. B. Ashcom *et al.*, J. Opt. Soc. Am. B **23**, 2317 (2006).
[17] R. Rankin *et al.*, Opt. Lett. **16**, 835 (1991).
[18] D. Romanov *et al.*, Opt. Lett. **32**, 3161 (2007).
[19] A. A. Fridman and L. A. Kennedy, *Plasma Physics and Engineering* (Taylor and Francis, New York, 2004).
[20] T. N. Rescigno *et al.*, Science **286**, 2474 (1999).
[21] P. L. Bartlett and A. T. Stelbovics, Phys. Rev. A **66**, 012707 (2002).
[22] W. Vanroose *et al.*, Science **310**, 1787 (2005).
[23] S. M. Younger and T. D. Mark, in *Electron Impact Ionization*, edited by T. D. Mark and G. H. Dunn (Springer-Verlag, Wien, New York, 1985), pp. 24.
[24] D. G. Steel and J. F. Lam, Opt. Lett. **4**, 363 (1979).